Tan et al. *Cell Discovery* (2022)8:50
https://doi.org/10.1038/s41421-022-00412-3

Cell Discovery
www.nature.com/celldisc

ARTICLE Open Access

Structural insights into the ligand binding and G_i coupling of serotonin receptor 5-HT_{5A}

Yangxia Tan[1,2], Peiyu Xu[1,3], Sijie Huang[1,2], Gong Yang[4], Fulai Zhou[1,3], Xinheng He[1,3], Honglei Ma[5], H. Eric Xu[1,2,3]✉ and Yi Jiang[1,2,6]✉

Abstract

5-hydroxytryptamine receptor 5A (5-HT_{5A}) belongs to the 5-HT receptor family and signals through the $G_{i/o}$ protein. It is involved in nervous system regulation and an attractive target for the treatment of psychosis, depression, schizophrenia, and neuropathic pain. 5-HT_{5A} is the only $G_{i/o}$-coupled 5-HT receptor subtype lacking a high-resolution structure, which hampers the mechanistic understanding of ligand binding and $G_{i/o}$ coupling for 5-HT_{5A}. Here we report a cryo-electron microscopy structure of the 5-HT_{5A}–G_i complex bound to 5-Carboxamidotryptamine (5-CT). Combined with functional analysis, this structure reveals the 5-CT recognition mechanism and identifies the receptor residue at 6.55 as a determinant of the 5-CT selectivity for $G_{i/o}$-coupled 5-HT receptors. In addition, 5-HT_{5A} shows an overall conserved G_i protein coupling mode compared with other $G_{i/o}$-coupled 5-HT receptors. These findings provide comprehensive insights into the ligand binding and G protein coupling of $G_{i/o}$-coupled 5-HT receptors and offer a template for the design of 5-HT_{5A}-selective drugs.

Introduction

5-hydroxytryptamine (5-HT) receptors are widely expressed in the central and peripheral nervous systems and are involved in a variety of psychiatric disorders. They are one of the most promising drug targets for the treatment of nervous system diseases[1]. There are seven distinct types (5-HT_{1-7}), comprised of 14 subtypes in the 5-HT receptor family, of which 13 are G protein-coupled receptors (GPCRs) (Fig. 1a). So far, 26 structures of 5-HT receptors have been reported, including crystal structures of 5-HT_{1B}[2,3], 5-HT_{2A}[4,5], 5-HT_{2B}[6–9], and 5-HT_{2C}[10], as well as cryo-electron microscopy (cryo-EM) structures of all members of 5-HT_1, including 5-HT_{1A}[11], 5-HT_{1B}[12], 5-HT_{1D}[11], 5-HT_{1E}[11], and 5-HT_{1F}[13], in complex with $G_{i/o}$ protein. These structures provide a basis for understanding ligand recognition and functional regulation of these 5-HT receptors. Besides 5-HT_1, 5-HT_5 is another type of $G_{i/o}$-coupled 5-HT receptor and also remains the last type of $G_{i/o}$-coupled 5-HT receptor without a reported structure.

The 5-HT_5 subfamily consists of two members, designated as 5-HT_{5A} and 5-HT_{5B}, which share 69% sequence identity with each other and have 23%–34% homology with other 5-HT receptors[14]. Of note, 5-HT_{5B} is the first example of a brain-specific receptor that is absent in humans, of which the coding sequence is interrupted by stop codons[14,15]. Thus, 5-HT_{5A} stands out as the only 5-HT_5 subtype expressed in human brain regions, including the cerebral cortex, hippocampus, and raphe nuclei[16,17]. 5-HT_{5A} shows an antinociceptive role and is involved in the regulation of memory, learning, and food intake[18,19]. Its specific ligands have shown potential in the treatment of psychosis, depression, schizophrenia, and neuropathic pain[20]. Thus, the development of 5-HT_{5A}-selective drugs will offer a new opportunity for the treatment of these nervous system diseases.

Correspondence: H Eric Xu (eric.xu@simm.ac.cn) or Yi Jiang (yijiang@simm.ac.cn)
[1]The CAS Key Laboratory of Receptor Research, Shanghai Institute of Materia Medica, Chinese Academy of Sciences, Shanghai, China
[2]School of Life Science and Technology, ShanghaiTech University, Shanghai, China
Full list of author information is available at the end of the article
These authors contributed equally: Yangxia Tan, Peiyu Xu, Sijie Huang

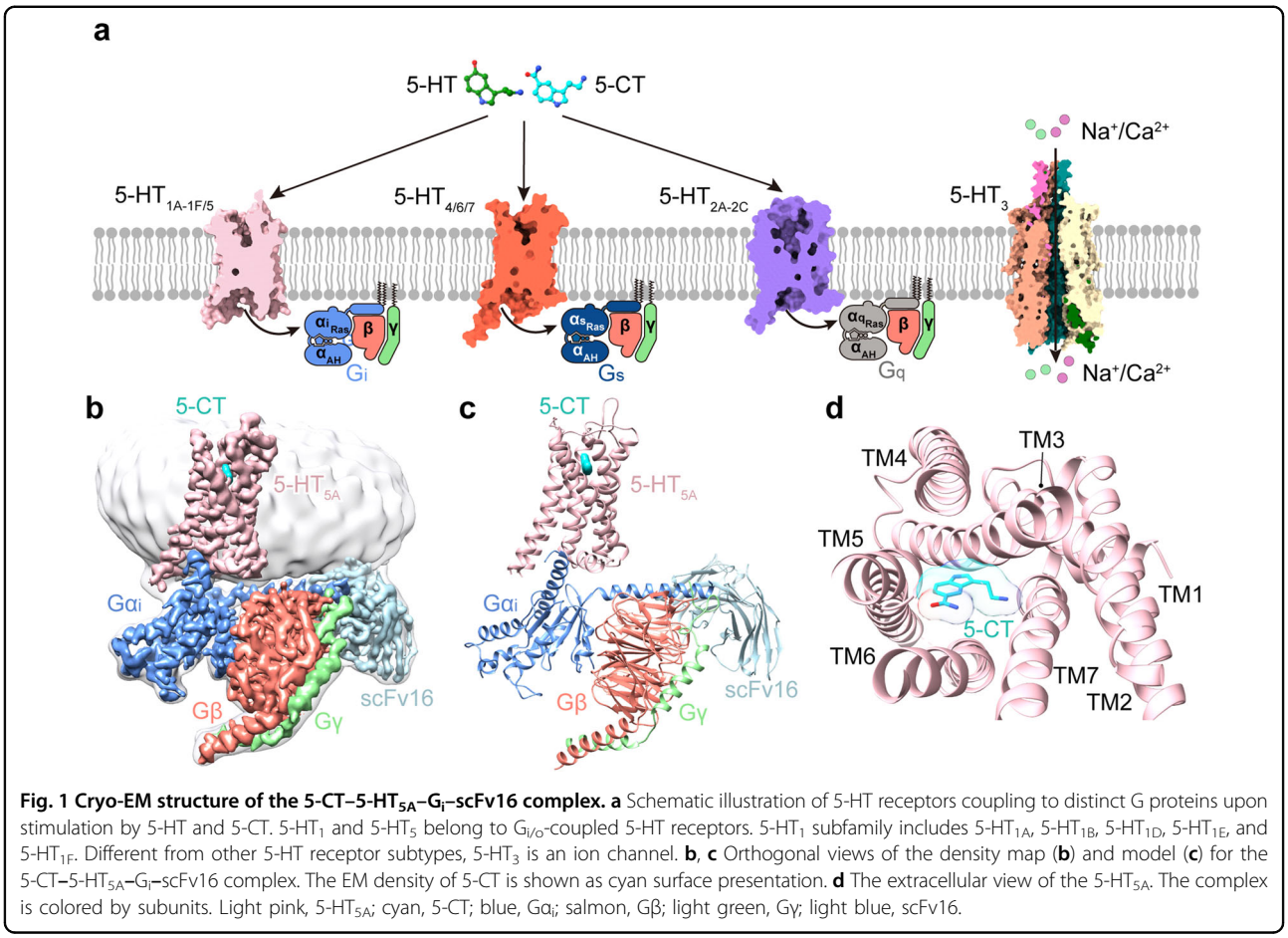

Fig. 1 Cryo-EM structure of the 5-CT–5-HT$_{5A}$–G$_i$–scFv16 complex. a Schematic illustration of 5-HT receptors coupling to distinct G proteins upon stimulation by 5-HT and 5-CT. 5-HT$_1$ and 5-HT$_5$ belong to G$_{i/o}$-coupled 5-HT receptors. 5-HT$_1$ subfamily includes 5-HT$_{1A}$, 5-HT$_{1B}$, 5-HT$_{1D}$, 5-HT$_{1E}$, and 5-HT$_{1F}$. Different from other 5-HT receptor subtypes, 5-HT$_3$ is an ion channel. **b**, **c** Orthogonal views of the density map (**b**) and model (**c**) for the 5-CT–5-HT$_{5A}$–G$_i$–scFv16 complex. The EM density of 5-CT is shown as cyan surface presentation. **d** The extracellular view of the 5-HT$_{5A}$. The complex is colored by subunits. Light pink, 5-HT$_{5A}$; cyan, 5-CT; blue, Gα$_i$; salmon, Gβ; light green, Gγ; light blue, scFv16.

However, the selective ligands for 5-HT$_{5A}$ are still lacking. 5-Carboxamidotryptamine (5-CT) is a synthetic agonist for 5-HT$_{5A}$ and also activates other G$_{i/o}$-coupled 5-HT receptors with distinct affinities. It shows a moderate affinity for 5-HT$_{5A}$ with a pK_i value of 7.7 and displays high affinities for 5-HT$_{1A}$, 5-HT$_{1B}$, and 5-HT$_{1D}$ (pK_i = 8.9–9.0)[21–25]. In contrast, 5-CT displays negligible affinities for 5-HT$_{1E}$ (pK_i = 5.4) and 5-HT$_{1F}$ (pK_i = 6.1) (https://pdsp.unc.edu/pdspweb/)[26,27]. SB699551 and ASP5736 stand out as two selective antagonists, which have been widely used for functional studies of 5-HT$_{5A}$[20,28]. The availability of the structure of ligand-bound 5-HT$_{5A}$ may accelerate the design of 5-HT$_{5A}$-targeting drugs by providing an accurate structure template.

In this study, we report the structure of G$_i$-coupled 5-HT$_{5A}$ complex bound to 5-CT at a resolution of 3.1 Å. This structure clarified the feature of 5-CT recognition by 5-HT$_{5A}$ and identified a determinant for 5-CT affinities against G$_{i/o}$-coupled 5-HT receptors, thus providing a rationale for designing drugs targeting 5-HT$_{5A}$. Structural comparison of the 5-HT$_{5A}$–G$_i$ with other G$_{i/o}$-coupled 5-HT receptor complexes deepens our understanding of the mechanism underlying ligand recognition and G$_{i/o}$ coupling.

Results

Cryo-EM structure of the 5-CT–5-HT$_{5A}$–G$_i$–scFv16 complex

We used the full-length human 5-HT$_{5A}$ for structural studies. A BRIL was fused to the N-terminus of 5-HT$_{5A}$ to improve expression. The NanoBiT tethering strategy was applied to stabilize the 5-HT$_{5A}$–G$_i$ complex, which had been widely used in the structure determination of several GPCR–G protein complexes[29–31] (Supplementary Fig. S1). The C-terminus of the receptor and the Gβ$_1$ subunit were connected to the LgBiT and HiBiT, respectively. A dominant-negative form of the human Gα$_{i1}$ mutant containing four mutations (S47N, G203A, E345A, and A326S), referred to as Gα$_{i1(4DN)}$, was applied[32]. The 5-HT$_{5A}$–G$_i$ complex was assembled by co-expressing the engineered receptor with Gα$_{i1(4DN)}$, Gβ$_1$, Gγ$_2$ subunits, and scFv16 in High Five (Hi5) cells in the presence of 5-CT.

The structure of the 5-CT–5-HT$_{5A}$–G$_i$–scFv16 complex was determined with an overall resolution of 3.1 Å (Fig. 1b, c; Supplementary Fig. S2 and Table S1). The high-quality density maps are clear for modeling 5-HT$_{5A}$ from residue 31 to residue 353, with the exception of residues 237–275 in the intracellular loop 3 (ICL3). The

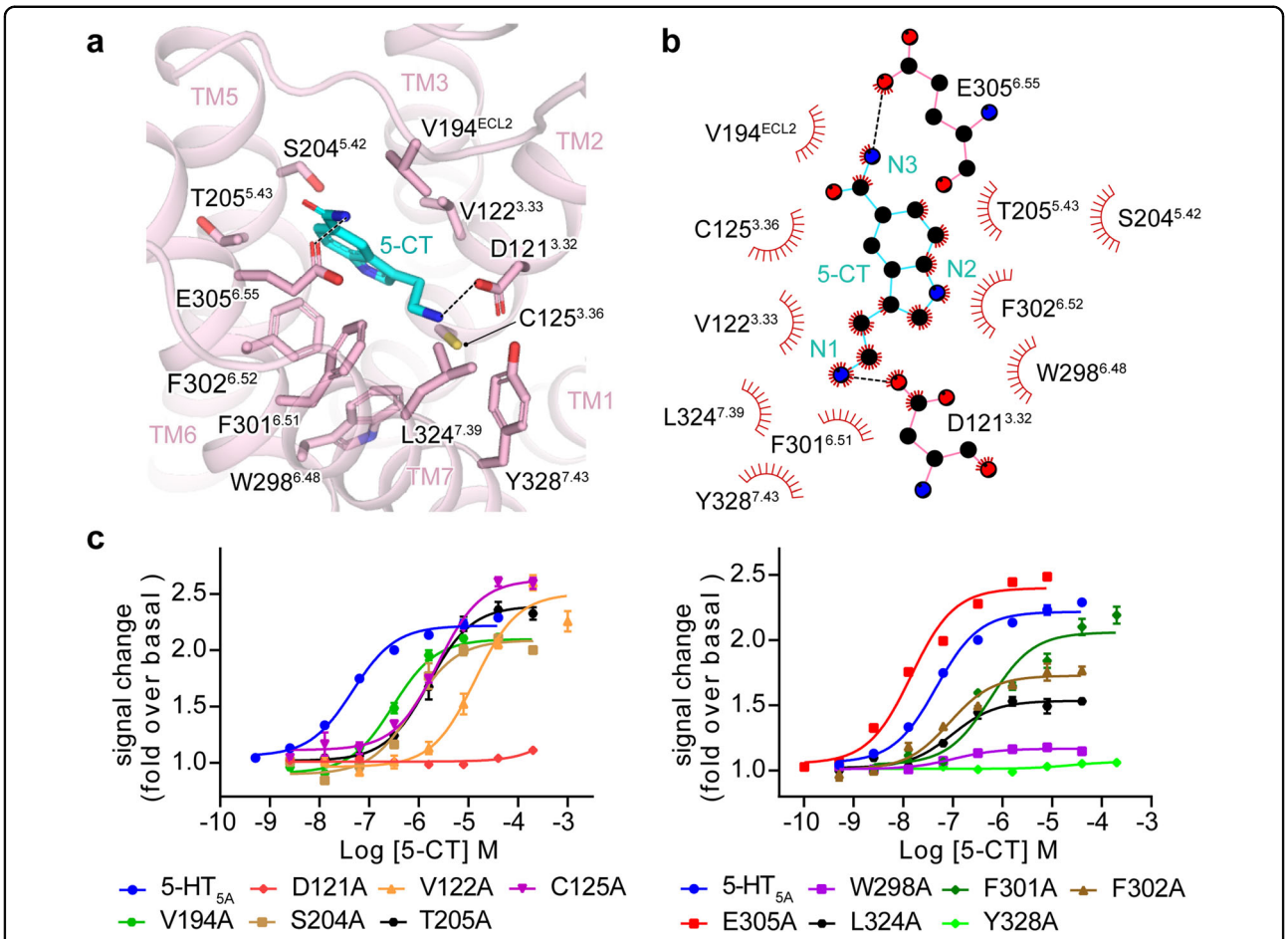

Fig. 2 The 5-CT-binding pocket of 5-HT$_{5A}$. a Detailed interactions of 5-CT with residues in the binding pocket of 5-HT$_{5A}$. **b** 2D schematic representation of interactions between 5-CT and residues in the ligand-binding pocket of 5-HT$_{5A}$, analyzed by LigPlot^{+} program. The polar interactions are indicated as black dashed lines. **c** Effects of alanine mutation of pocket residues of 5-HT$_{5A}$ on 5-CT-induced G$_i$ protein recruitment. Three independent NanoBiT assays in triplicates were performed. Each data point presents mean ± SEM from a representative experiment.

majority of the residue side chains in the seven-transmembrane helical domain (TMD), three extracellular loops (ECL1–ECL3), and two ICLs (ICL1 and ICL2) of 5-HT$_{5A}$ were well-defined. 5-CT, scFv16, and the three subunits of G$_i$ protein are also well-fitted in the EM map. The entire model provides detailed structural information on the 5-CT-binding pocket and 5-HT$_{5A}$–G$_i$ interaction interface (Fig. 1c, d; Supplementary Fig. S3).

The recognition of G$_{i/o}$-coupled 5-HT receptors by agonists

The binding pocket in 5-HT$_{5A}$ is largely overlapped with that in other G$_{i/o}$-coupled 5-HT receptors, sharing 11 of 16 identical residues. 5-CT is embedded deep into the pocket constituted by TM3, ECL2, and TM5–TM7 of 5-HT$_{5A}$ (Fig. 2a). Compared with other ligands bound to G$_{i/o}$-coupled 5-HT receptors, 5-CT adopts a similar binding pose in 5-HT$_{5A}$ (Supplementary Fig. S4a). Its indole scaffold is anchored through a salt bridge between its positively charged nitrogen at the 3-aminoethyl group and the carboxylate of D121$^{3.32}$ (Fig. 2a, b). This salt bridge is highly conserved across ligand-bound 5-HT receptors with known structures (Supplementary Fig. S4b). Mutating D121$^{3.32}$ to alanine abolished the 5-CT-induced 5-HT$_{5A}$ activation, highlighting its importance to 5-CT activity (Fig. 2c). In addition, the side chain of D121$^{3.32}$ is further stabilized by an intramolecular hydrogen bond between D121$^{3.32}$ and Y328$^{7.43}$, which is supported by the alanine mutagenesis data. On the other side, the nitrogen at the 5-carboxamide of 5-CT forms a hydrogen bond with the side chain of E305$^{6.55}$. Besides polar interactions, the indole scaffold of 5-CT tightly packs against a hydrophobic cleft comprising side chains of V122$^{3.33}$, F301$^{6.51}$, F302$^{6.52}$, and L324$^{7.39}$. These hydrophobic residues substantially contribute to 5-CT-induced 5-HT$_{5A}$ activation (Fig. 2c; Supplementary Table S2).

It has been thought that the ligand-binding pocket of each G$_{i/o}$-coupled 5-HT receptor is comprised of two

subpockets, the orthosteric binding pocket (OBP) and the extended binding pocket (EBP)[2,8]. OBP of $G_{i/o}$-coupled 5-HT receptors locates deep into the core of the TMD pocket, whereas the EBP approaches the extracellular surface of the entire binding pocket (Supplementary Fig. S4a). The 11 conserved residues in the binding pocket across $G_{i/o}$-coupled 5-HT receptors are located in the OBP, including $D^{3.32}$, $C^{3.36}$, $T^{3.37}$, $I^{4.56}$, $S^{5.42}$, $T^{5.43}$, $A^{5.46}$, $W^{6.48}$, $F^{6.51}$, $F^{6.52}$, and $Y^{7.43}$ (Supplementary Fig. S4b), of which $D^{3.32}$ is thought critical to ligand binding for 5-HT and other monoamine receptors by forming a conserved salt bridge with the basic cyclic amine of ligands[2]. The featured benzene ring of the ligand is surrounded by conserved hydrophobic residues in $G_{i/o}$-coupled 5-HT receptors, including $W^{6.48}$, $F^{6.51}$, $F^{6.52}$, and $Y^{7.43}$. This hydrophobic environment is crucial for ligand-induced receptor activation. Inspection of the binding poses of ligands in $G_{i/o}$-coupled 5-HT receptors reveals that 5-HT, 5-CT, and BRL54443 only occupy the OBP. In contrast, Donitriptan and Lasmiditan, two anti-migraine drugs selectively targeting 5-$HT_{1B/1D}$ and 5-HT_{1F}, respectively, are relatively bulky and occupy both OBP and EBP of specific receptors (Supplementary Fig. S4a). These structural observations are consistent with the contention that OBP is critical to the binding potency of ligands, whereas the EBP plays a predominant role in determining ligand selectivity[2]. Together, these findings provide insights into the 5-CT recognition for 5-HT_{5A} and deepen our understanding of ligand selectivity for 5-HT receptors.

Role of the residue at 6.55 in the determination of 5-CT selectivity for $G_{i/o}$-coupled 5-HT receptors

5-CT shows different selectivity for $G_{i/o}$-coupled 5-HT receptors. It exhibits high affinities for 5-HT_{1A}, 5-HT_{1B}, and 5-HT_{1D} ($pK_i = 7.9–8.1$) and relatively weak affinities for 5-HT_{1E}, 5-HT_{1F}, and 5-HT_{5A} ($pK_i = 5.4–7.0$) (Fig. 3b; Supplementary Table S3). Sequence comparison of residues in the EBP of $G_{i/o}$-coupled 5-HT receptors reveals a low sequence identity at position 6.55 (Supplementary Fig. S4b). The residue at 6.55 is alanine in 5-HT_{1A} and serine in 5-HT_{1B} and 5-HT_{1D}. In contrast, the cognate residue in 5-HT_{1E}, 5-HT_{1F}, and 5-HT_{5A} is glutamic acid. The difference in residue composition raises a hypothesis that the residue at 6.55 is involved in 5-CT selectivity for $G_{i/o}$-coupled 5-HT receptors.

To prove this hypothesis, we introduced swap mutations to residues at 6.55 across $G_{i/o}$-coupled 5-HT receptors. Our G_i protein recruitment data support two-facet roles of the residue at 6.55 in 5-CT-induced receptor activation. One is the steric hindrance arising from the side chain of the residue at position 6.55 (Fig. 3c). For 5-HT_{1A}, $A365^{6.55}E$ and $A365^{6.55}S$ mutations, which increase the size of the side chain, reduced 5-CT-induced receptor activation relative to the WT receptor. $S334^{6.55}E$ mutation of 5-HT_{1B} decreased 5-CT activity, while substituting the serine with a smaller side chain residue alanine dramatically increased 5-CT potency. Similarly, mutating glutamic acid of 5-HT_{1E} and 5-HT_{5A} to alanine or serine, two residues with a relatively small side chain, notably promoted receptor activation. These findings corroborate the idea that the bulkier side chain of glutamic acid relative to alanine and serine may prevent the binding of 5-CT and receptor activation through steric hindrance. On the other hand, 5-CT may form hydrogen bonds with the glutamic acid at 6.55 in $G_{i/o}$-coupled 5-HT receptors, which may dominate the ligand–receptor interaction over the hindrance effects of the side chain (Fig. 3c). This point is supported by functional analysis of 5-HT_{1D} and 5-HT_{1F}. $S321^{6.55}E$ mutation of the 5-HT_{1D} enhanced 5-CT activity, despite the increased side-chain size. Consistently, $E313^{6.55}S$ and $E313^{6.55}A$ mutations in 5-HT_{1F} almost abolished 5-CT activity. Thus, residues at position 6.55 modulate the activity of $G_{i/o}$-coupled 5-HT receptors through two aspects of roles: the steric hindrance effects for 5-HT_{1A}, 5-HT_{1B}, 5-HT_{1E}, and 5-HT_{5A} and the hydrogen bond-forming capacity as an acceptor for 5-HT_{1D} and 5-HT_{1F}. Together, our findings provide further evidence for the previous speculation that the residue at 6.55 is responsible for the ligand-recognition specificity of 5-HT receptors and offer a new opportunity for the design of drugs selectively targeting 5-HT receptors[11].

General features of the activation and G protein coupling of $G_{i/o}$-coupled 5-HT receptors

Similar to agonists bound to other $G_{i/o}$-coupled 5-HT receptors, 5-CT directly contacts the toggle switch residue $W^{6.48}$ of 5-HT_{5A} and triggers its rotameric switch. The change of $W^{6.48}$ initiates the rotation and outward movement of the TM6 cytoplasmic end of 5-HT_{5A} relative to inverse agonist-bound 5-HT_{1B} (PDB: 5V54), the hallmark of class A GPCR activation (Fig. 4a, b).

Structural comparison of the G_i-coupled 5-HT_{5A} with other $G_{i/o}$-coupled 5-HT receptors whose structures had been solved revealed an almost overlapped receptor activation conformation. However, the α5 helices of $G\alpha_{i/o}$ subunits in these 5-HT receptor complexes showed slight tilts to different extents, which cause rotation of the entire $G_{i/o}$ proteins, leading to the most noticeable translational movement of the αN helices (Fig. 4a). The global coupling interface profile analysis showed that the majority of the $G\alpha_i$ subunit-interacting residues in TM3, ICL2, TM5, TM6, TM7, and helix 8 are conserved across $G_{i/o}$-coupled 5-HT receptors, including $R^{3.50}$, $I^{3.54}$, $I^{5.61}$, $A^{5.65}$, $R/K^{6.29}$, $R/K^{6.32}$, and $N^{8.47}$. Differently, no substantial interactions were seen between ICL3 of $G_{i/o}$-coupled 5-HT receptors and G_i protein, with an exception of 5-HT_{1D}, which shows an additional EM density of ICL3 and a more extensive ICL3–G_i interaction[11] (Fig. 4c).

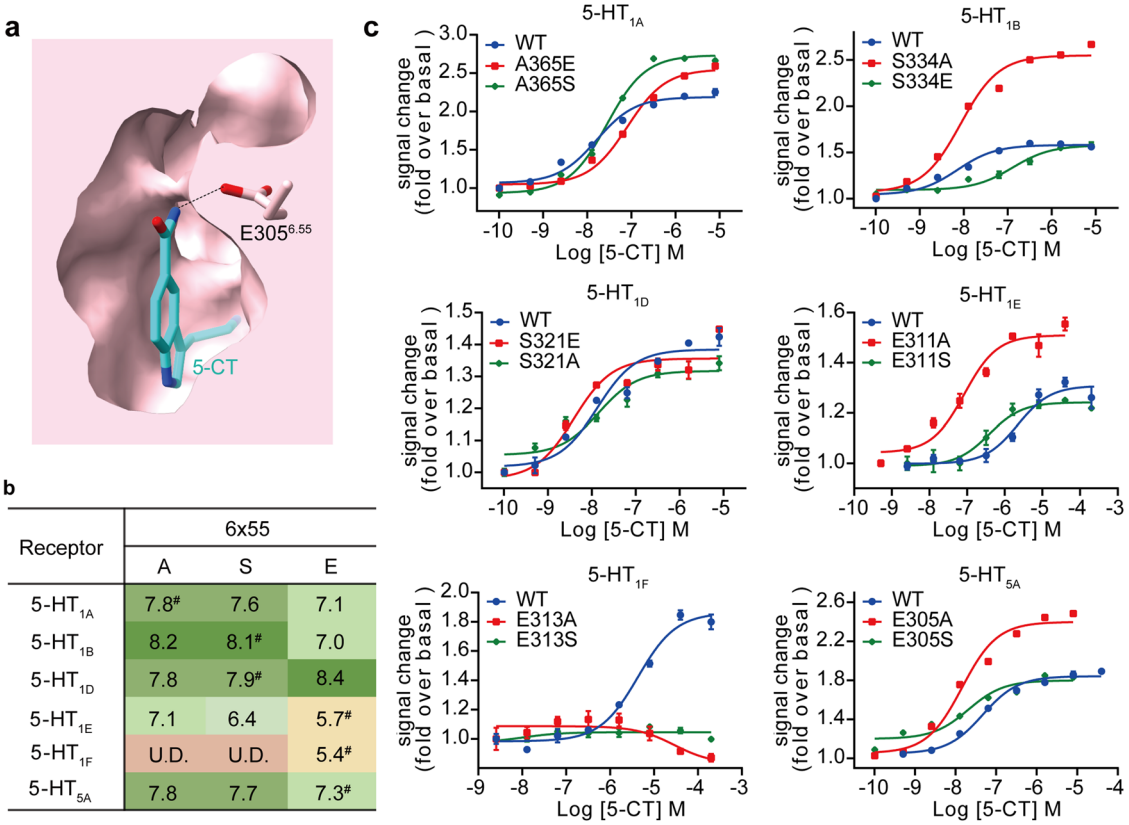

Receptor	6x55		
	A	S	E
5-HT$_{1A}$	7.8#	7.6	7.1
5-HT$_{1B}$	8.2	8.1#	7.0
5-HT$_{1D}$	7.8	7.9#	8.4
5-HT$_{1E}$	7.1	6.4	5.7#
5-HT$_{1F}$	U.D.	U.D.	5.4#
5-HT$_{5A}$	7.8	7.7	7.3#

Fig. 3 Role of the residue at 6.55 in determining 5-CT selectivity of $G_{i/o}$-coupled 5-HT receptors. a Cross-section of the orthosteric binding pocket of 5-HT$_{5A}$. The hydrophobic interaction between 5-CT and E305$^{6.55}$ is indicated as a black dashed line. **b** 5-CT activity (pEC$_{50}$ values) for wild-type (WT) and mutants of $G_{i/o}$-coupled 5-HT receptors. #5-CT activity (pEC$_{50}$ values) for WT receptors. U.D., undetectable. **c** Effects of mutations at 6.55 on 5-CT-induced G_i protein recruitment of $G_{i/o}$-coupled receptors. Three independent NanoBiT assays in triplicates were performed. Each data point presents mean ± SEM from a representative experiment.

Two major interfaces exist between 5-HT$_{5A}$ and G_i protein. The cytoplasmic receptor cavity constituted by TM3, TM5, TM6, and the TM7–helix 8 junction accommodates the distal C-terminal end of the α5 helix of the Gα$_i$ subunit, forming a primary interface (Fig. 4d). The residues of α5 helix hydrophobically contact the receptor cavity. L348, C351, L353, and F354 in the α5 helix of the Gα$_i$ subunit contact a hydrophobic patch comprised of residues in TM3 (I143$^{3.54}$), TM5 (I223$^{5.61}$, A227$^{5.65}$, and V231$^{5.69}$), and TM6 (A283$^{6.33}$ and V287$^{6.37}$). In addition, residues R230$^{5.68}$ and S233$^{5.71}$ of TM5 form well-defined hydrogen bonds with D341 and K345 from the α5 helix, respectively (Fig. 4d). The ICL2 also interacts with Gα$_i$, constituting the other major interface. M147$^{34.51}$ of ICL2 inserts into the groove constituted by hydrophobic residues in the α5 helix, the β1 and β3 strands, and αN of the Gα$_i$ subunit. A hydrogen bond present between R152$^{34.56}$ and E28 may further stabilize the ICL2–Gα$_i$ interface (Fig. 4e). Together, these findings clarify the activation and G_i coupling features of 5-HT$_{5A}$ and provide a comprehensive understanding of the G protein coupling mechanism of $G_{i/o}$-coupled 5-HT receptors.

Discussion

5-HT$_{5A}$ is a $G_{i/o}$-coupled 5-HT receptor subtype and is involved in nervous system disorders, thus serving as an important drug target. It is the only $G_{i/o}$-coupled 5-HT receptor subtype lacking a high-resolution structure to date. In this paper, we report a 3.1 Å-resolution cryo-EM structure of the 5-HT$_{5A}$–G_i complex bound to a synthetic agonist, 5-CT, which is also the first 5-CT-bound 5-HT receptor structure. Our structure reveals the recognition mechanism of 5-HT$_{5A}$ by 5-CT and adds to the pool of the structures for deepening our understanding of the ligand-binding mode of 5-HT receptors. Furthermore, structural comparison and functional analysis of the ligand-binding pockets reveal that the residue at 6.55 serves as a determinant for the 5-CT specificity for $G_{i/o}$-coupled 5-HT receptors. This ligand specificity is partly attributed to the steric hindrance arising from the

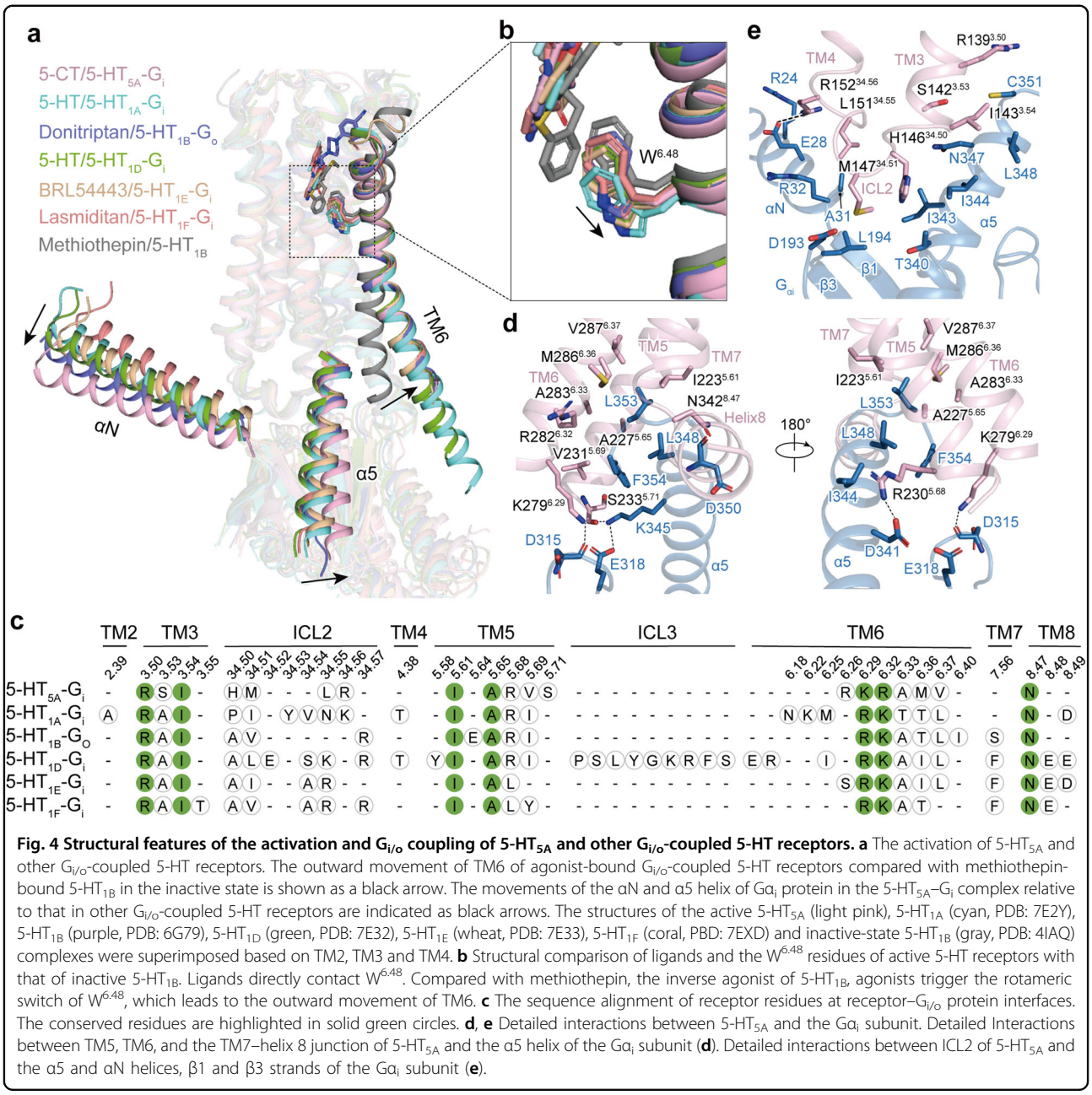

Fig. 4 Structural features of the activation and $G_{i/o}$ coupling of 5-HT_{5A} and other $G_{i/o}$-coupled 5-HT receptors. a The activation of 5-HT_{5A} and other $G_{i/o}$-coupled 5-HT receptors. The outward movement of TM6 of agonist-bound $G_{i/o}$-coupled 5-HT receptors compared with methiothepin-bound 5-HT_{1B} in the inactive state is shown as a black arrow. The movements of the αN and α5 helix of $G\alpha_i$ protein in the 5-HT_{5A}–G_i complex relative to that in other $G_{i/o}$-coupled 5-HT receptors are indicated as black arrows. The structures of the active 5-HT_{5A} (light pink), 5-HT_{1A} (cyan, PDB: 7E2Y), 5-HT_{1B} (purple, PDB: 6G79), 5-HT_{1D} (green, PDB: 7E32), 5-HT_{1E} (wheat, PDB: 7E33), 5-HT_{1F} (coral, PBD: 7EXD) and inactive-state 5-HT_{1B} (gray, PDB: 4IAQ) complexes were superimposed based on TM2, TM3 and TM4. **b** Structural comparison of ligands and the $W^{6.48}$ residues of active 5-HT receptors with that of inactive 5-HT_{1B}. Ligands directly contact $W^{6.48}$. Compared with methiothepin, the inverse agonist of 5-HT_{1B}, agonists trigger the rotameric switch of $W^{6.48}$, which leads to the outward movement of TM6. **c** The sequence alignment of receptor residues at receptor–$G_{i/o}$ protein interfaces. The conserved residues are highlighted in solid green circles. **d**, **e** Detailed interactions between 5-HT_{5A} and the $G\alpha_i$ subunit. Detailed Interactions between TM5, TM6, and the TM7–helix 8 junction of 5-HT_{5A} and the α5 helix of the $G\alpha_i$ subunit (**d**). Detailed interactions between ICL2 of 5-HT_{5A} and the α5 and αN helices, β1 and β3 strands of the $G\alpha_i$ subunit (**e**).

side chain of the residue at 6.55 or its potential polar interaction with ligands. In addition, our structure reveals a similar activation mechanism and an overall conserved G_i protein coupling mode for 5-HT_{5A} compared with other $G_{i/o}$-coupled 5-HT receptors. These findings broaden our understanding of ligand recognition in the 5-HT system.

Although 5-HT_{5A} has been cloned for ~3 years, it is still one of the less well-characterized receptors in the 5-HT receptor family. The lack of selective ligands has delayed the functional studies on 5-HT_{5A} until the discovery of the selective antagonists SB699551 and ASP5736, which have improved our understanding of the localization of 5-HT in the brain and its function. However, it should be noted that we are still far from fully understanding the pharmacological characteristics of 5-HT_{5A}. Meanwhile, no drugs targeting 5-HT_{5A} have been registered for clinical trials or approved. Recently, virtual screening based on a homology model identified UCSF678, a 42 nM new chemical probe with partial agonism activity for 5-HT_{5A}. USCF678 exhibits enhanced selectivity for 5-HT_{5A} and a more restricted off-target profile than the existing 5-HT_{5A} antagonist SB699551. Unlike the promiscuous ligand 5-HT, molecular docking reveals that

USCF678 extends into the upper region of the binding pocket, known as EBP. $W117^{3.28}$ in EBP of 5-HT_{5A} is further proved to be responsible for the high-affinity binding of UCSF638, and the tryptophan at position 3.28 may contribute to the off-target binding of UCSF638 analogs[33]. These findings are consistent with the two pockets (OBP and EBP) binding model[2,8] and highlight the importance of EBP to the discovery of selective ligands. Consequently, the 5-HT_{5A} structure provides an accurate template for the rational design of drugs targeting 5-HT_{5A} and may offer a new opportunity for the treatment of nervous system diseases, including psychosis, depression, schizophrenia, and neuropathic pain.

Materials and methods

Constructs

The human full-length 5-HT_{5A} was cloned into the pFastBac with an N-terminal haemagglutinin (HA) sequence followed by a Flag-tag, 15× His-tag, BRIL-tag, and a LgBiT sequence at the C-terminus to facilitate the protein expression and purification. The human $G\alpha_i$ with four dominant-negative mutations, S47N, G203A, E245A, and A326S was applied. Human $G\beta_1$, human $G\gamma_2$, and scFv16 were cloned into pFastBac vector using homologous recombination (ClonExpress One Step Cloning Kit, Vazyme).

Expression and complex purification

5-HT_{5A}-LgBiT, DN_$G\alpha_i$, $G\beta_1$-SmBiT, $G\gamma_2$, and scFv16 were co-expressed in Hi5 insect cells (Invitrogen) using the Bac-to-Bac baculovirus expression system (ThermoFisher). Cell cultures were grown in ESF 921 medium (Expression Systems) to a density of 3×10^6 cells/mL, and then infected with five separate baculoviruses, respectively, at the ratio of 1:1:1:1:1.5. The culture was harvested by centrifugation 48 h post-infection and stored at −80 °C for further usage.

Cell pellets were lysed in 20 mM HEPES, pH 7.4, 20 mM KCl, 10 mM $MgCl_2$, 5 mM $CaCl_2$, and 10% glycerol supplemented with Protease Inhibitor Cocktail (TargetMol). The 5-HT_{5A}–G_i complex was formed on the membrane for 1.5 h at room temperature by addition of 10 μM 5-CT and 25 mU/mL apyrase (Sigma), and then solubilized from the membrane by using 0.5% (w/v) *n*-dodecyl-β-D-maltoside (DDM) (Anatrace) and 0.1% (w/v) cholesteryl hemisuccinate (CHS) (Anatrace) for 2 h at 4 °C, followed by centrifugation at 85,000 × *g* for 30 min to extract the solubilized complex. The supernatant was subsequently incubated by nickel affinity chromatography (Ni Smart Beads 6FF, SMART Lifesciences) at 4 °C for 3 h. The resin was washed with 20 column volumes of the buffer containing 20 mM HEPES, pH 7.4, 100 mM NaCl, 25 mM imidazole, 0.01% (w/v) LMNG (Anatrace), 0.005% GDN (Anatrace), 0.004% (w/v) CHS (Anatrace), and 5 μM 5-CT. The complex was then eluted with six column volumes of the same buffer containing 300 mM imidazole. The protein was concentrated and subjected onto a Superdex 200 Increase 10/300 column (GE Healthcare) in the buffer containing 20 mM HEPES, pH 7.4, 100 mM NaCl, 0.00075% (w/v) LMNG (Anatrace), 0.00025% (w/v) GDN (Anatrace), 0.0002% (w/v) CHS (Anatrace) and 10 mM 5-CT. The purified complex fractions were collected and concentrated for cryo-EM experiments.

Cryo-EM grid preparation and data collection

For the cryo-EM grid preparation, 3 μL of the purified 5-CT–5-HT_{5A}–G_i complex at a final concentration of 25 mg/mL was applied to glow-discharged holey carbon grids (Quantifoil R1.2/1.3, 300 mesh), and vitrified using a Vitrobot Mark IV (ThermoFisher Scientific) subsequently. Grids were plunge-frozen in liquid ethane using Vitrobot Mark IV (Thermo Fischer Scientific). Frozen grids were transferred to liquid nitrogen and stored for data acquisition. Cryo-EM images were collected by an FEI Titan Krios at 300 kV accelerating voltage equipped with a Gatan K3 Summit direct electron detector at the Center of Cryo-Electron Microscopy Research Center, Shanghai Institute of Materia Medica, Chinese Academy of Sciences (Shanghai, China). A total of 5303 movies were automatically acquired using SerialEM10 in super-resolution counting mode at a pixel size of 1.071 Å. The images were recorded at a dose rate of about 26.7 e/$Å^2$/s with a defocus ranging from −1.2 to −2.2 μm. The total exposure time was 3 s, and intermediate frames were recorded in 0.083-s intervals, resulting in a total of 36 frames per micrograph.

Image processing and 3D reconstruction

Image stacks were subjected to beam-induced motion correction using MotionCor2.1[34], while contrast transfer function (CTF) parameters were determined by Gctf[35]. Automated particle selection and data processing were performed using Relion 3.0[36]. Automated particle selection yielded 3,767,450 particles. The particles were subjected to reference-free 2D classification, producing 1,327,660 particles with well-defined averages. The map of 5-HT_{1E}–G_i–scFv16 complex (EMDB-30975)[11] low-pass filtered to 40 Å was used as an initial reference model for 3D classification, which produced two good subsets showing clear structural features accounting for 754,854 particles. These particles were subsequently subjected to Bayesian polishing, CTF refinement, and 3D refinement, which generated a map with an indicated global resolution of 3.1 Å at a Fourier shell correlation of 0.143. Local resolution was determined using the Resmap[37] with half maps as input maps.

Model building and refinement

The cryo-EM structure of the 5-CT–5-HT_{5A}–G_i complex (PDB: 7E2Y) and the G_i protein model (PDB: 6DDE)

were used to generate the initial model and refinement against the electron microscopy map. The model was docked into the EM density map using UCSF Chimera[38], followed by iterative manual adjustment and rebuilding in COOT[39] and ISOLDE[40] according to side-chain densities. Real-space refinement was performed using Phenix programs[41]. The model statistics were validated using MolProbity[42]. Structural figures were prepared in Chimera, ChimeraX[43], and PyMOL (https://pymol.org/2/). The final refinement statistics are provided in Supplementary Table S1.

NanoBiT G protein recruitment assay

NanoBiT, a NanoLuc luciferase-based method, is used to detect the interaction between receptor and G protein in living cells[44]. The full-length 5-HT_{5A} was fused with a LgBiT fragment (17.6 kDa) at its C-terminus via a 15-amino acid flexible linker. SmBiT, a 13-amino acid peptide, was C-terminally fused to the Gβ subunit using the same linker. The cDNAs of 5-HT_{5A}-LgBiT, $G\alpha_{i1}$, $G\beta_1$-SmBiT, and $G\gamma_2$ were cloned into pFastBac vector (Invitrogen). The baculoviruses were prepared using the bac-to-bac system (Invitrogen). Hi5 cells were cultured in ESF 921 medium (Expression Systems) to a density of 2.5–3 million cells per mL and then infected with four separate baculoviruses at the ratio of 1:1:1:1. After 48 h infection, the culture was collected by centrifugation, and the cell pellet was resuspended with PBS. The cell suspension was seeded onto 384-well microtiter plates (40 μL per well) and loaded with 5 μL of 50 μM coelenterazine (Yeasen) diluted in the assay buffer. 5 μL of ligands were added and incubated for 3–5 min at room temperature before measurement. Luminescence counts were normalized to the initial count to show the G protein binding response.

Surface expression analysis

Cell surface expression for each mutant was monitored using flow cytometry. The expressed Hi5 cells (10 μL) were incubated with 10 μL anti-FLAG-FITC antibody (Sigma), which is diluted with PBS containing 4% BSA at a final ratio of 1:1000, at 4 °C for 15 min, and 180 μL 1× PBS was then added to the cells. The surface expression of each mutant was monitored by detecting the fluorescent intensity of FITC using a BD ACCURI C6.

Acknowledgements

The Cryo-EM data of the 5-CT–5-HT_{5A}–G_i complex were collected at the Cryo-Electron Microscopy Research Center, Shanghai Institute of Material Medica. We thank all the staff at the cryo-EM facilities for their technical support. This work was partially supported by the National Natural Science Foundation (32171187 to Y.J., 82121005 to Y.J., and H.E.X., 32130022 to H.E.X.); the Ministry of Science and Technology (China) grants (2018YFA0507002 to H.E.X.); the Shanghai Municipal Science and Technology Major Project (2019SHZDZX02 to H.E.X.); Shanghai Municipal Science and Technology Major Project (H.E.X.); the CAS Strategic Priority Research Program (XDB37030103 to H.E.X.); Shandong University (Qilu Young Scholar 62450082163091 to H.M.); Shanghai Municipal Science and Technology Commission (19ZR1467500 to H.M.); the Young Innovator Association of CAS Enrollment (H.M.).

Author details

[1]The CAS Key Laboratory of Receptor Research, Shanghai Institute of Materia Medica, Chinese Academy of Sciences, Shanghai, China. [2]School of Life Science and Technology, ShanghaiTech University, Shanghai, China. [3]University of Chinese Academy of Sciences, Beijing, China. [4]State Key Laboratory of Cellular Stress Biology, School of Life Sciences, Xiamen University, Xiamen, Fujian, China. [5]State Key Laboratory of Microbial Technology, Shandong University, Qingdao, Shandong, China. [6]Lingang Laboratory, Shanghai, China

Author contributions

Y.T. and P.X. optimized the conditions of protein samples for final structure determination; Y.T. and S.H. generated the expression constructs and optimized the 5-HT_{5A}–G_i protein complex; Y.T. purified the protein samples for final structure determination, participated in cryo-EM grid inspection, data collection, model building, executed the functional assay, and prepared the figures and manuscript draft; P.X. evaluated the specimen by negative-stain EM, screened the cryo-EM conditions, prepared the cryo-EM grids, collected cryo-EM images, and refined the structures; G.Y. participated in the functional assay; F.Z. analyzed the interactions between 5-HT_{5A} and 5-CT by LigPlot$^+$ program; X.H. and H.M. participated in structure analysis and model building. Y. J. participated in the supervision of Y.T., S.H., P.X., X.H., and F.Z., analyzed the structures, prepared the figures, and edited the manuscript. H.E.X. and Y.J. conceived and supervised the project, and wrote the manuscript with inputs from all authors.

Data availability

The atomic coordinate and the electron microscopy map for the 5-CT–5-HT_{5A}–G_i–scFv16 complex have been deposited in the Protein Data Bank (PDB) under accession number 7X5H and Electron Microscopy Data Bank (EMDB) under accession number EMD-33014, respectively.

Conflict of interest

The authors declare no competing interests.

Publisher's note

Springer Nature remains neutral with regard to jurisdictional claims in published maps and institutional affiliations.

Supplementary information The online version contains supplementary material available at https://doi.org/10.1038/s41421-022-00412-3.

Received: 16 November 2021 Accepted: 12 April 2022
Published online: 24 May 2022

References

1. Berger, M., Gray, J. A. & Roth, B. L. The expanded biology of serotonin. *Annu. Rev. Med.* **60**, 355–366 (2009).
2. Wang, C. et al. Structural basis for molecular recognition at serotonin receptors. *Science* **340**, 610–614 (2013).
3. Yin, W. et al. Crystal structure of the human 5-HT1B serotonin receptor bound to an inverse agonist. *Cell Discov.* **4**, 12 (2018).
4. Kimura, K. T. et al. Structures of the 5-HT2A receptor in complex with the antipsychotics risperidone and zotepine. *Nat. Struct. Mol. Biol.* **26**, 121–128 (2019).
5. Kim, K. et al. Structure of a hallucinogen-activated Gq-coupled 5-HT2A serotonin receptor. *Cell* **182**, 1574–1588.e19 (2020).
6. Wacker, D. et al. Structural features for functional selectivity at serotonin receptors. *Science* **340**, 615–619 (2013).
7. Ishchenko, A. et al. Structural insights into the extracellular recognition of the human serotonin 2B receptor by an antibody. *Proc. Natl. Acad. Sci. USA* **114**, 8223–8228 (2017).
8. McCorvy, J. D. et al. Structural determinants of 5-HT2B receptor activation and biased agonism. *Nat. Struct. Mol. Biol.* **25**, 787–796 (2018).

9. Wacker, D. et al. Crystal structure of an LSD-bound human serotonin receptor. *Cell* **168**, 377–389.e12 (2017).
10. Peng, Y. et al. 5-HT2C receptor structures reveal the structural basis of GPCR polypharmacology. *Cell* **172**, 719–730.e14 (2018).
11. Xu, P. et al. Structural insights into the lipid and ligand regulation of serotonin receptors. *Nature* **592**, 469–473 (2021).
12. Garcia-Nafria, J., Nehme, R., Edwards, P. C. & Tate, C. G. Cryo-EM structure of the serotonin 5-HT1B receptor coupled to heterotrimeric Go. *Nature* **558**, 620–623 (2018).
13. Huang, S. et al. Structural basis for recognition of anti-migraine drug lasmiditan by the serotonin receptor 5-HT1F-G protein complex. *Cell Res.* **31**, 1036–1038 (2021).
14. Grailhe, R., Grabtree, G. W. & Hen, R. Human 5-HT(5) receptors: the 5-HT(5A) receptor is functional but the 5-HT(5B) receptor was lost during mammalian evolution. *Eur. J. Pharm.* **418**, 157–167 (2001).
15. Nelson, D. L. 5-HT5 receptors. *Curr. Drug Targets CNS Neurol. Disord.* **3**, 53–58 (2004).
16. Kassai, F. et al. Effect of 5-HT5A antagonists in animal models of schizophrenia, anxiety and depression. *Behav. Pharm.* **23**, 397–406 (2012).
17. Thomas, D. R. 5-ht5A receptors as a therapeutic target. *Pharm. Ther.* **111**, 707–714 (2006).
18. Vidal-Cantu, G. C. et al. Role of 5-HT5A and 5-HT1B/1D receptors in the antinociception produced by ergotamine and valerenic acid in the rat formalin test. *Eur. J. Pharm.* **781**, 109–116 (2016).
19. Lopez-Esparza, S., Berumen, L. C., Padilla, K., Miledi, R. & Garcia-Alcocer, G. Expression of hippocampal serotonin receptors 5-HT2C and 5-HT5A in a rat model of diet-induced obesity supplemented with tryptophan. *Int J. Dev. Neurosci.* **42**, 80–85 (2015).
20. Yamazaki, M. et al. ASP5736, a novel 5-HT5A receptor antagonist, ameliorates positive symptoms and cognitive impairment in animal models of schizophrenia. *Eur. Neuropsychopharmacol.* **24**, 1698–1708 (2014).
21. Leysen, J. E. et al. Alniditan, a new 5-hydroxytryptamine1D agonist and migraine-abortive agent: ligand-binding properties of human 5-hydroxytryptamine1D alpha, human 5-hydroxytryptamine1D beta, and calf 5-hydroxytryptamine1D receptors investigated with [3H]5-hydroxytryptamine and [3H]alniditan. *Mol. Pharm.* **50**, 1567–1580 (1996).
22. Newman-Tancredi, A. et al. Agonist activity of antimigraine drugs at recombinant human 5-HT1A receptors: potential implications for prophylactic and acute therapy. *Naunyn Schmiedebergs Arch. Pharm.* **355**, 682–688 (1997).
23. Newman-Tancredi, A. et al. Agonist and antagonist actions of antipsychotic agents at 5-HT1A receptors: a [35S]GTPgammaS binding study. *Eur. J. Pharm.* **355**, 245–256 (1998).
24. Parker, E. M., Izzarelli, D. G., Lewis-Higgins, L., Palmer, D. & Shapiro, R. A. Two amino acid differences in the sixth transmembrane domain are partially responsible for the pharmacological differences between the 5-HT1D beta and 5-HT1E 5-hydroxytryptamine receptors. *J. Neurochem.* **67**, 2096–2103 (1996).
25. Rees, S. et al. Cloning and characterisation of the human 5-HT5A serotonin receptor. *FEBS Lett.* **355**, 242–246 (1994).
26. McAllister, G. et al. Molecular cloning of a serotonin receptor from human brain (5HT1E): a fifth 5HT1-like subtype. *Proc. Natl. Acad. Sci. USA* **89**, 5517–5521 (1992).
27. Adham, N. et al. Cloning of another human serotonin receptor (5-HT1F): a fifth 5-HT1 receptor subtype coupled to the inhibition of adenylate cyclase. *Proc. Natl. Acad. Sci. USA* **90**, 408–412 (1993).
28. Thomas, D. R. et al. SB-699551-A (3-cyclopentyl-N-[2-(dimethylamino)ethyl]-N-[(4'-[[(2-phenylethyl)amino]methyl]-4 -biphenylyl)methyl]propanamide dihydrochloride), a novel 5-ht5A receptor-selective antagonist, enhances 5-HT neuronal function: evidence for an autoreceptor role for the 5-ht5A receptor in guinea pig brain. *Neuropharmacology* **51**, 566–577 (2006).
29. Duan, J. et al. Cryo-EM structure of an activated VIP1 receptor-G protein complex revealed by a NanoBiT tethering strategy. *Nat. Commun.* **11**, 4121 (2020).
30. Yin, Y. L. et al. Molecular basis for kinin selectivity and activation of the human bradykinin receptors. *Nat. Struct. Mol. Biol.* **28**, 755–761 (2021).
31. Wang, Y. et al. Molecular recognition of an acyl-peptide hormone and activation of ghrelin receptor. *Nat. Commun.* **12**, 5064 (2021).
32. Liu, P. et al. The structural basis of the dominant negative phenotype of the Galphai1beta1gamma2 G203A/A326S heterotrimer. *Acta Pharm. Sin.* **37**, 1259–1272 (2016).
33. Levit Kaplan, A. et al. Structure-based design of a chemical probe set for the 5-HT5A serotonin receptor. *J. Med. Chem.* https://doi.org/10.1021/acs.jmedchem.1c02031 (2022).
34. Zheng, S. Q. et al. MotionCor2: anisotropic correction of beam-induced motion for improved cryo-electron microscopy. *Nat. Methods* **14**, 331–332 (2017).
35. Zhang, K. Gctf: Real-time CTF determination and correction. *J. Struct. Biol.* **193**, 1–12 (2016).
36. Scheres, S. H. RELION: implementation of a Bayesian approach to cryo-EM structure determination. *J. Struct. Biol.* **180**, 519–530 (2012).
37. Heymann, J. B. Guidelines for using Bsoft for high resolution reconstruction and validation of biomolecular structures from electron micrographs. *Protein Sci.* **27**, 159–171 (2018).
38. Pettersen, E. F. et al. UCSF Chimera–a visualization system for exploratory research and analysis. *J. Comput. Chem.* **25**, 1605–1612 (2004).
39. Emsley, P. & Cowtan, K. Coot: model-building tools for molecular graphics. *Acta Crystallogr. D Biol. Crystallogr.* **60**, 2126–2132 (2004).
40. Croll, T. I. ISOLDE: a physically realistic environment for model building into low-resolution electron-density maps. *Acta Crystallogr. D Struct. Biol.* **74**, 519–530 (2018).
41. Adams, P. D. et al. PHENIX: a comprehensive Python-based system for macromolecular structure solution. *Acta Crystallogr. D Biol. Crystallogr.* **66**, 213–221 (2010).
42. Chen, V. B. et al. MolProbity: all-atom structure validation for macromolecular crystallography. *Acta Crystallogr. D Biol. Crystallogr.* **66**, 12–21 (2010).
43. Pettersen, E. F. et al. UCSF ChimeraX: structure visualization for researchers, educators, and developers. *Protein Sci.* **30**, 70–82 (2021).
44. Xu, P. et al. Structures of the human dopamine D3 receptor-Gi complexes. *Mol. Cell* **81**, 1147–1159.e44 (2021).